

BALLOON OBSERVATIONS OF AURORAL X-RAYS AT ESRANGE, SWEDEN AND RELATED PHENOMENA

YO HIRASIMA, HIROYUKI MURAKAMI, KIYOAKI OKUDAIRA,
*Department of Physics, Rikkyo University, 34-1, Nishi-Ikebukuro 3-chome,
Toshima-ku, Tokyo 171*

MASAMI FUJII, JUN NISHIMURA, TAKAMASA YAMAGAMI,
*The Institute of Space and Astronautical Science, 6-1, Komaba 4-chome,
Meguro-ku, Tokyo 153*

MASAKI EJIRI, HIROSHI MIYAOKA, TAKAYUKI ONO
National Institute of Polar Research, 9-10, Kaga 1-chome, Itabashi-ku, Tokyo 173

and

MASAHIRO KODAMA
Department of Physics, Yamanashi Medical College, Tamaho, Nakakoma, Yamanashi 409-38

Abstract: Balloon observations of auroral X-rays using different detector systems were carried out twice over Esrangle, Sweden, in November and December 1982, in order to examine spatial and temporal characteristics of the energetic component of auroral electrons. One detector is a telescope system consisting of four scintillation counters whose fields of view are different with each other as well as with the viewing directions. It is shown from the first flight carrying the telescope system that a limited illuminating region of auroral X-rays coincides with that of visual aurora. The other is the so-called pinhole camera and a shot of X-ray image detected by a thin NaI (Tl) crystal is viewed by a microchannel plate photomultiplier tube (MCP PMT) with 4×4 anodes. The second flight was made for simultaneous observations by three kinds of payloads of the MCP PMT system, a subsidiary X-ray energy counter and a VLF wave receiver. The balloon did not encounter good activity of aurora enough for X-ray image-formings by the MCP PMT system during the ceiling flight, but the other two detectors revealed the first on-board evidence of the auroral X-ray event well associated with abrupt absorption of VLF emissions.

1. Introduction

Since auroral X-rays detectable at balloon altitudes reflect the most energetic phenomenon in the magnetosphere, morphological and dynamical studies of them are of great importance as a direct information on the primary precipitating high-energy electrons during polar magnetic substorms. The auroral X-rays with energies of the order of ten keV are produced in the upper atmosphere by the bremsstrahlung of more energetic electrons which are possibly accelerated deeper in the magneto-

sphere (PARKS *et al.*, 1977). On the other hand, the low-energy electrons dominant in the visual aurorae are believed to be accelerated by the field-aligned electric fields near the earth (LIN and HOFFMAN, 1979; MOZER, 1980). Therefore, the inter-comparison of the illuminating regions between optical emissions and X-rays is of interest in terms of the spatial and temporal characteristics.

In most cases of auroral breakups, visual aurorae scarcely exhibit the uniform illuminating pattern over the whole sky but they appear partly accompanying fine and complex structures. As an X-ray detector is capable to take a wide dynamic range of counting rates, it is easy to identify a possible illuminating region of X-rays with high time and spatial resolutions, though it depends on the size of auroral activity. Indeed, several balloon observations for determining the spatial distributions of auroral X-rays have been made by using the directional telescope system of detector (PARKS, 1967; YAMAGAMI *et al.*, 1978) or the pinhole camera system (MAUK *et al.*, 1981). Also, some rocket experiments were performed for the purpose of mapping auroral X-rays (KODAMA and OGUTI, 1976; GOLDBERG *et al.*, 1982).

Two balloons carrying either one of the two kinds of X-ray image-forming detectors were launched from ESRANGE, Sweden, on November 23 and December 9, 1982, respectively. This balloon campaign is the second step following the first Japan-Sweden-Norway international cooperative work of March 1982, in which a close relation between auroral X-ray microbursts and VLF emissions was investigated (YAMAGISHI *et al.*, 1984).

One of the X-ray detectors used in the present campaign is a counter telescope type consisting of four NaI (Tl) scintillation detectors, each of which has different view-fields and view-directions. The other one is a new X-ray pinhole camera developed by HIRASIMA *et al.* (1983), which comprises a 16-anode microchannel plate photomultiplier tube (denoted by MCP PMT hereafter) coupled to a thin NaI (Tl) crystal. Unfortunately, both of the flights did not encounter aurorae intense enough to discriminate fine structures of auroral X-ray images. However, the counter telescope system observed an X-ray illuminating region coincident with a visual auroral region. Also a single X-ray counter with an energy spectrometer and an on-board VLF receiver presented the first evidence of a small X-ray enhancement associated with absorption of VLF emissions. Observation results obtained from these two flights are described and discussed.

2. Instrumentation

2.1. Directional telescope system

The arrangement of the balloon-borne four X-ray telescopes is shown in Fig. 1. Their fields of view and directions of sight projected on the celestial sphere are shown in Fig. 2. Each telescope uses a NaI (Tl) crystal of 1'' (diameter) \times 3 mm (thickness). A cylindrical collimator attached to the crystal consists of double layers of a lead sheet of 1 mm thickness and a tin sheet of 2 mm thickness, and determines the geometry of the individual view-field.

The vertical counter A always looks in the zenith direction with half cone angle of 30°. The field of view of the inclined counter B is limited to half view-field of counter

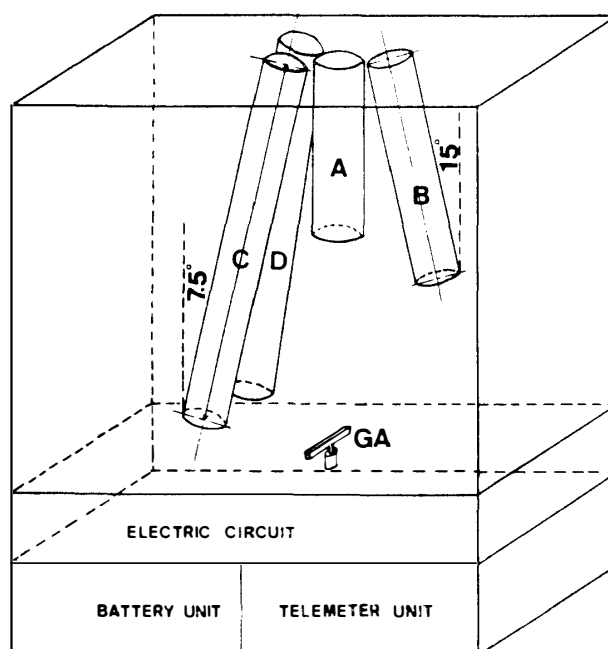


Fig. 1. Arrangement of four X-ray counters, one vertical (A) and three inclined (B, C, D), on-board a balloon B₁₅-2N. GA means a geomagnetic aspect sensor.

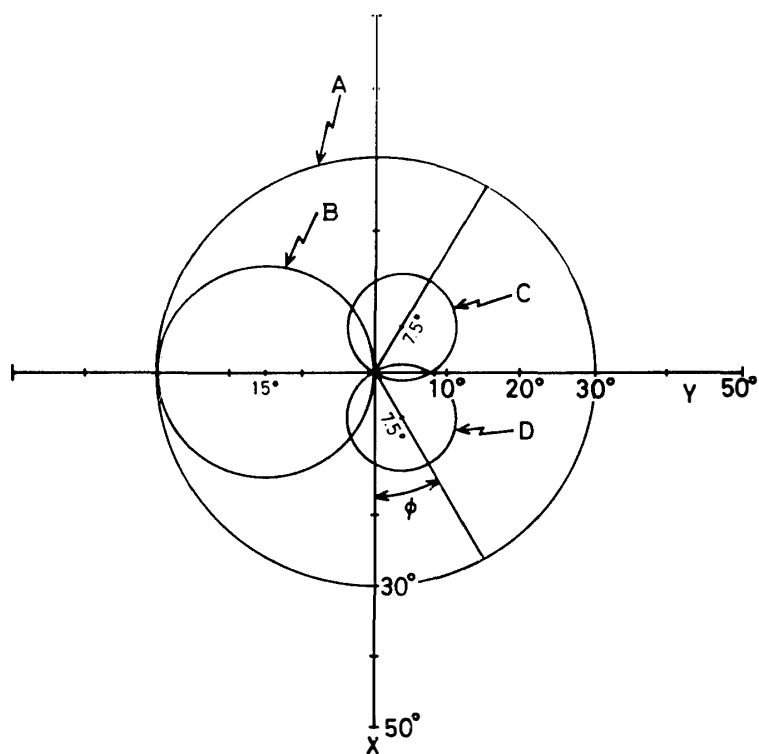


Fig. 2. Fields of view and directions of sight for the four X-ray counters.

A and its central direction of sight is inclined 15° from the zenith, so as to recognize the azimuthal distribution of X-rays. The half cone angle of counters C and D having the same view-field is narrowest, being 7.5° . The three inclined counters, B,

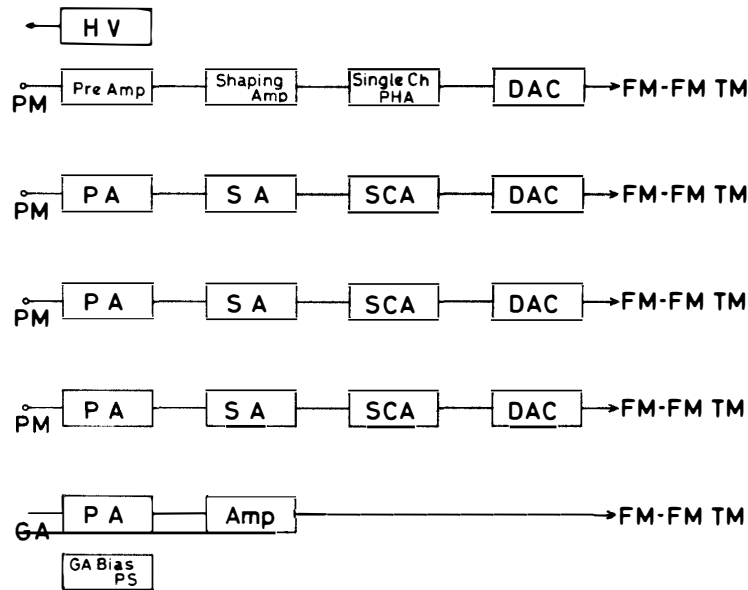


Fig. 3. Block diagram of the electronic system for the four X-ray counters (PM) and the aspect meter (GA).

C and D, are arranged with the azimuthal separation angles of 120° from each, as seen in Fig. 2.

The payload gondola is rotated by the motor drive at a constant speed of 3 rpm around the vertical axis, so that the azimuthal surveys by a set of three inclined counters are performed every 20 s. The measurable range of the X-ray energy is taken from 20 to 150 keV. A block diagram of the electronic circuits for the recording system is shown in Fig. 3. Digital count signals from an X-ray counter are converted into a superposed analogue pattern of double triangle shapes which contain a number of steps in one-to-one correspondence with counts. Eight descending steps follow 8 ascending steps and thus totally 16 steps, corresponding to 16 counts, constitute one small triangle. The next triangle pattern starts with a little level shift from the preceding one. Hence, a large triangle composed of 64 small triangles corresponds to 1024 counts. Examples of the double triangle pattern are shown in Fig. 4. Even

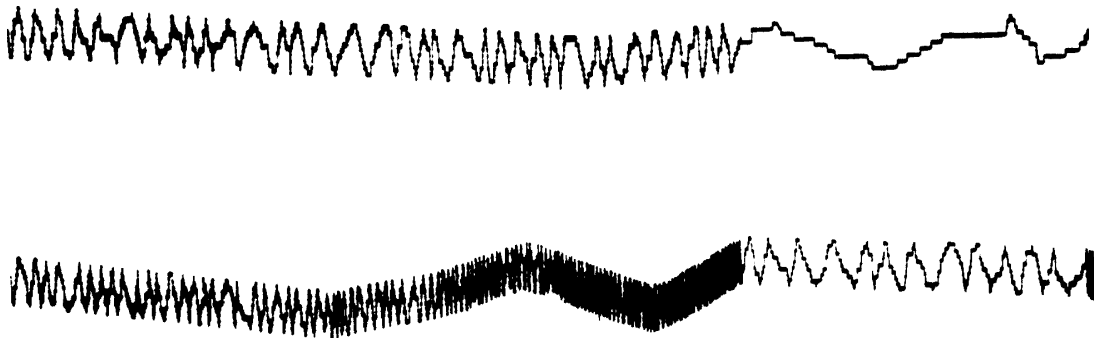


Fig. 4. Analogue pattern of the signal output from an X-ray counter, which is transmitted by the FM/FM telemetry. It consists of double triangle waves: the first order of triangle contains 16 steps, corresponding to 16 counts, and the second order of triangle contains 64 first-order triangles, which corresponds to 1024 counts.

if it happens to raise very high counting rates due to intense X-ray bursts, the number of the large triangles can correctly give the real counting rates, as long as the FM/FM telemeter response is allowable. Thus a wide dynamic range of counting rates is confirmed.

2.2. Microchannel plate photomultiplier tube system

A configuration of the X-ray detector using the MCP PMT is shown in Fig. 5. This is a pinhole camera type of image detector. An X-ray image on a thin NaI (Tl) crystal of $3''\phi \times 3$ mm is transported to a photocathode of the MCP PMT through the optical guide consisting of 49 pieces of plastic square rods. The MCP PMT used here is Hamamatsu TV R1224 having 4×4 anodes, leading us to an auroral X-ray image composed by 4×4 pixels. This image detector has a full view-field of 44.5° and the angular resolution of 16.7° per pixel.

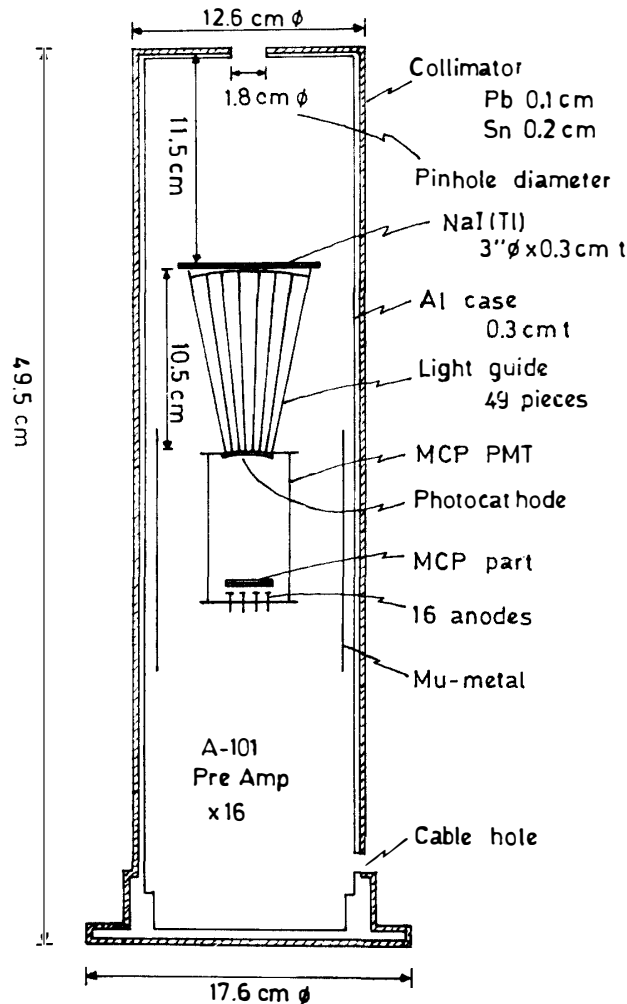


Fig. 5. Construction of the X-ray image detector using a microchannel plate photomultiplier tube (MCP PMT). An X-ray image on a NaI (Tl) crystal is sent by 7×7 pieces of plastic square rods of light guide into the photocathode of the MCP PMT, by which 4×4 pixels of the image are read out. All optical and electronic parts are completely shielded by a double layer slab of lead and tin, except a 'pinhole' on the top of the cylindrical aluminum container.

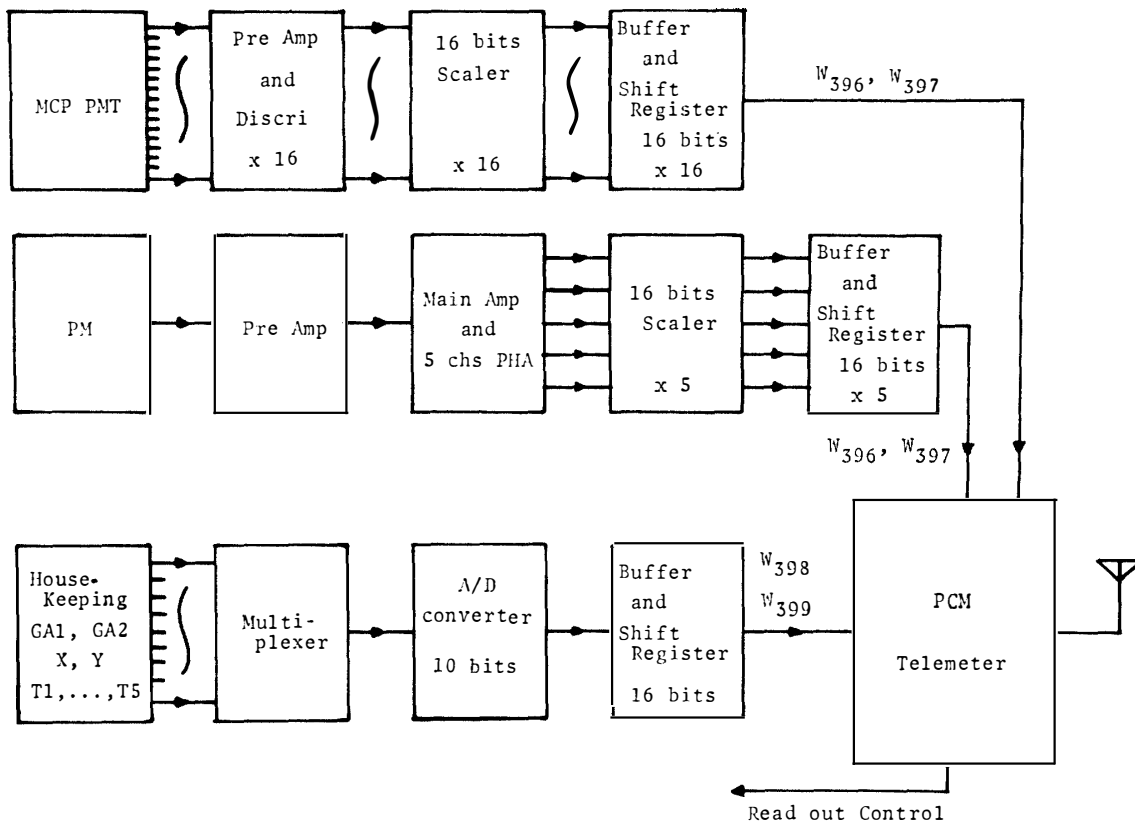


Fig. 6. Block diagram of the electronic assembly for the MCP PMT type of X-ray image detector, including the single X-ray energy counter and housekeeping system.

The minimum time resolution from one image to the next is decided by the PCM telemetry of $8 \text{ bits} \times 2 \text{ word} \times 500 \text{ minor frames}$ available for X-ray observations, the read-out time being 0.24 s during which the next data accumulation is in progress. An apparent image pattern can be arbitrarily deduced by adding successive 0.24-s basic data in the laboratory.

As one subsidiary observation, an omnidirectional X-ray scintillation counter ($1''\phi \times 3 \text{ mm NaI (Tl)}$, 145° opening cone toward the zenith) was prepared to measure the X-ray energy spectrum by the different five energy channels: 18–33, 33–60, 60–110, 110–200 keV and above 200 keV. A block diagram of the electronic circuits is shown in Fig. 6, where the housekeeping system such as temperatures, azimuth and horizontal level is included.

3. Observation Results

The first balloon, B₁₅-2N, carrying the four-telescope system of auroral X-ray image detector floated at a ceiling altitude of 10 mb from Esrangle toward the east-northeast direction during about six hours from 2059 UT of November 23 to 0336 UT of November 24, 1982. A moderate X-ray event was observed at 2256:30 to 2300:00 UT and recorded a peak value at 2257:20 UT, when the counting rate of counter A was about 10 times the background. Time profiles of counting rates of

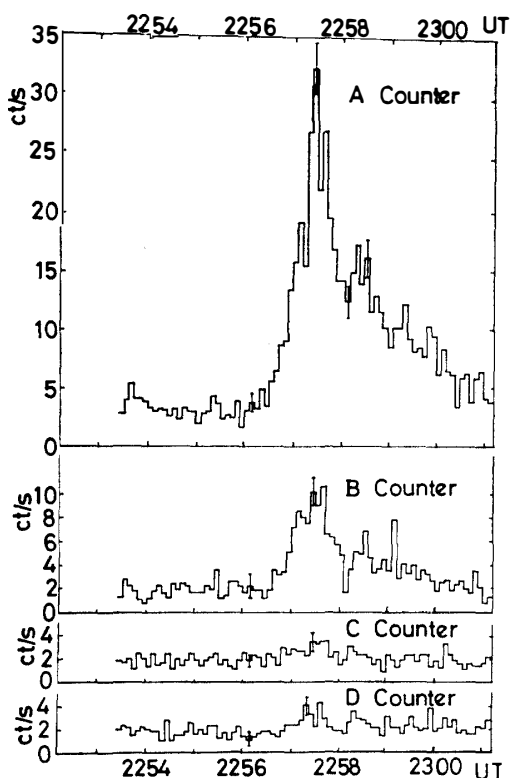


Fig. 7. Time profiles of 6-s counts from the four X-ray counters A, B, C and D in the flight of November 23, 1982.

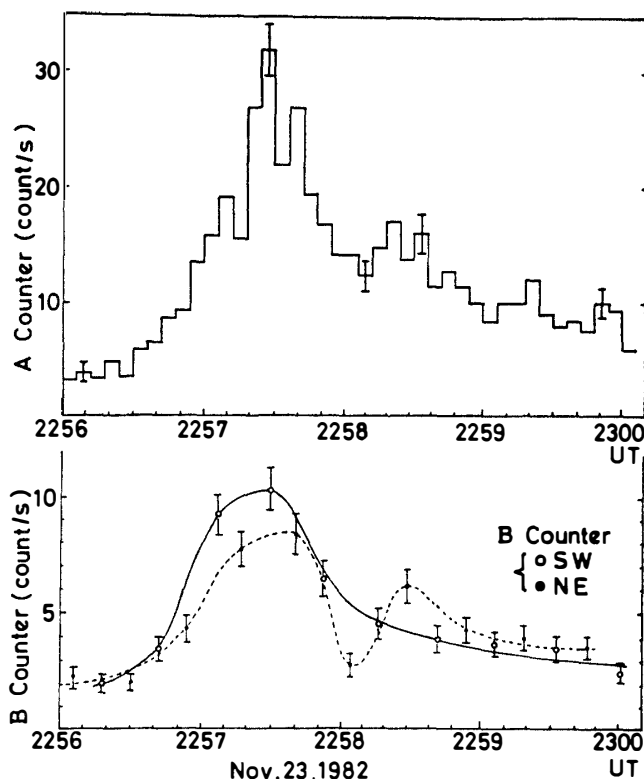


Fig. 8. Variations of the counting rates from the inclined counter B averaged for each of two hemispheres of SW and NE, where a slight fluctuation of the rotation speed of the gondola is taken into account. For comparison, the counting rates from the omnidirectional counter A are reproduced in the upper part.

the four X-ray counters are shown in Fig. 7. The inclined counter B can give the azimuthal distribution of counting rates with better statistical accuracy than in the others. Time profiles of counting rates of counter B for different half hemispheres directed to the southwest and the northeast respectively are shown in the lower portion of Fig. 8, where 6-s counts of counter A are again plotted for comparison. Hereafter we use SW and NE for these half hemispheres. It is evident that the counting rates of counter B viewing the SW are significantly higher than those for the NE during a small interval of 2256:50 to 2257:40 UT, when the counting rate of counter A reaches a peak value. Namely, auroral X-rays coming from the SW are predominant at this time interval.

Both the MCP PMT image detector and the energy spectral counter were flown by a balloon, B₁₅-4N, at 1715 to 2145 UT of December 9, 1982. The ceiling altitude is 11 mb. Unfortunately, no auroral breakup events were observed during the flight, but a small X-ray event was observed in the lower energy channels. A time profile of counting rates from the lowest energy channel (18–33 keV) is shown in Fig. 9, in which a small increase is found around 2050 UT on December 9, 1982. The corresponding slight increases are also seen in the next two higher energy channels.

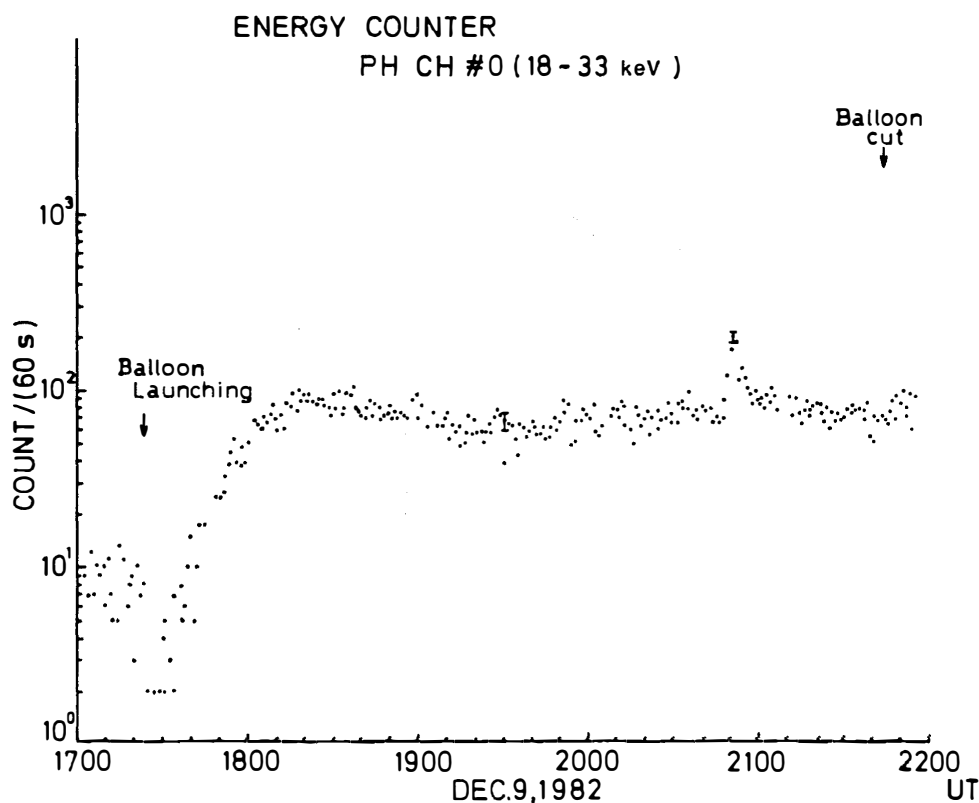


Fig. 9. Time profile of 1-min counting rates from the lowest X-ray energy channel (18-33 keV) during the entire balloon flight of December 9, 1982. A small increase is apparent around 2050 UT.

The energy spectra for the background and the enhanced X-rays are shown in Fig. 10, where the spectrum of the enhanced X-rays corrected for absorption in the residual atmosphere is shown. The corrected spectrum is approximated by a power law of $E_x^{-3.5}$ (E_x : X-ray energy).

4. Discussion and Conclusion

As seen in Fig. 8, auroral X-rays observed on November 23, 1982 are dominant in the southwest half hemisphere at 2256:50-2257:40 UT. Two photographs of visual aurorae taken by the all-sky camera at Esrange are shown in Fig. 11. A small circle marked in a left-upper part of the right-hand photograph taken at 2257:06 UT indicates the view-field of counter A at this moment. A spot within the circle indicates the zenith direction viewed from the balloon location. White areas seen in the photograph correspond to brilliant auroral regions. At 2256:06 UT, that is, one minute before, all of the X-ray counters showed the background counts and no brilliant aurorae appeared within the view-field of the vertical counter A, as seen in the left-hand photograph of Fig. 11 (the field of view is almost the same between the two moments). At 2257:06 UT, the brilliant auroral region appears in the southwest half of the view-field of counter A, when the counting rates of counter B are larger in the SW than in the NE, as seen in Fig. 8. After 2258:06 UT, visual auroral regions

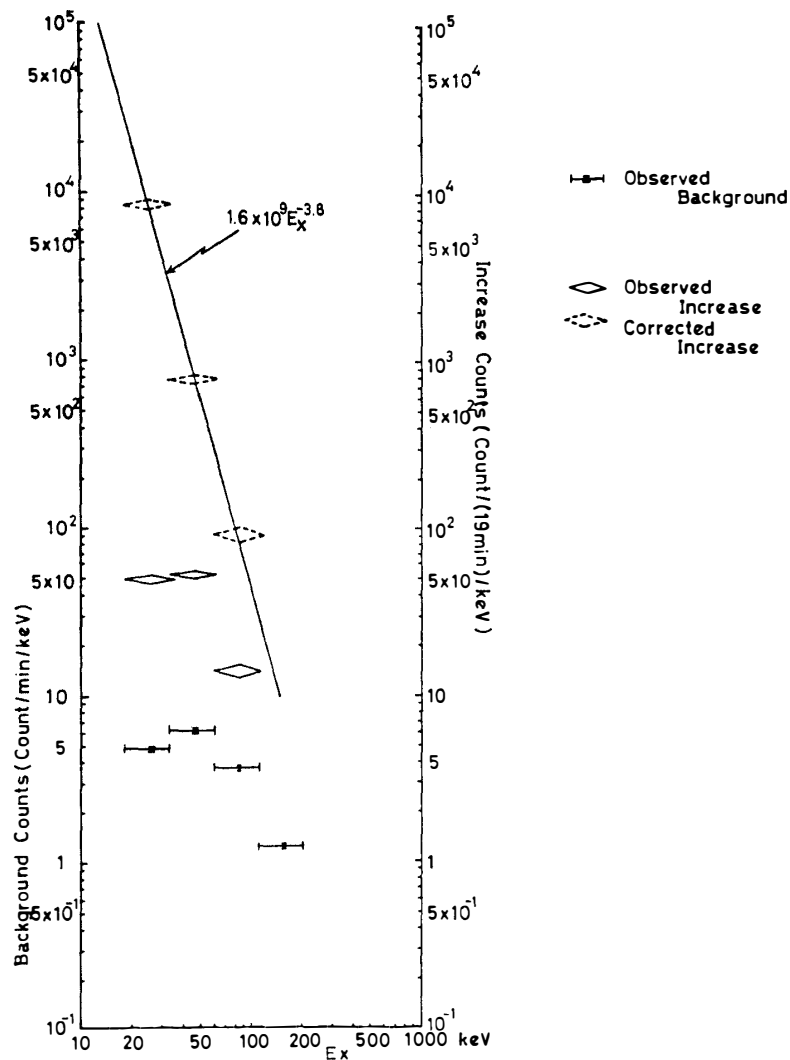


Fig. 10. Energy spectra of the auroral X-ray event of Fig. 9 and the background. The former is based on 19-min data sampling. Broken diamond symbols show the spectrum corrected for the residual atmosphere over the balloon altitude.

spread wider inside the view-field of counter A, while counting rates of counter A are increasing. It is, therefore, mentioned that the illuminating region of auroral X-rays almost coincides with that of visual aurora. Moreover, the movement of the X-ray illuminating region with time is similar to that of visual aurora, though it is within a limited part of the sky. It is suggested that both the low-energy electrons responsible for visual aurora and the high-energy electrons generating the bremsstrahlung X-rays precipitate simultaneously into the same region at this time interval.

On December 9, 1982, a slight increase of X-ray flux was observed at 2045–2107 UT, as shown in Fig. 9. During the balloon flight, on-board observations of VLF emissions (0.05–10 kHz) often showed emission enhancements with better improved S/N ratio than in the ground observation, particularly for the chorus waves of 3–4 kHz (ONO *et al.*, 1984). Dynamic spectra of VLF emissions observed at 2000–2145 UT interval are shown in Fig. 12, where dark parts show stronger emissions. The

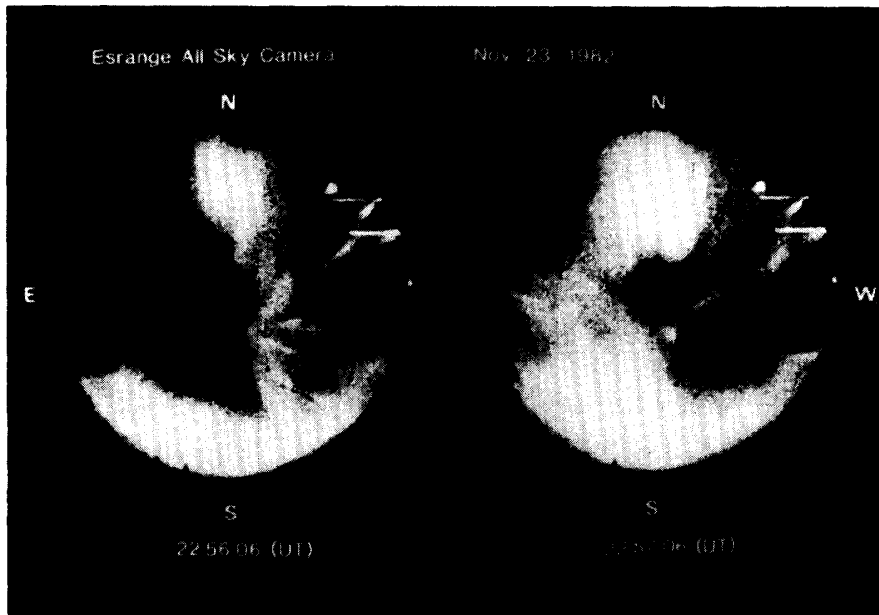


Fig. 11. All-sky camera photographs of aurora at Esrange. A small circle marked in the left-upper quadrant of the right-hand photograph indicates the field of view of the omnidirectional X-ray counter A. At 2257:06 UT half of the view-field is illuminated by brilliant aurora, but visual aurorae are out of the view-field before one minute, as seen in the left-hand photograph.

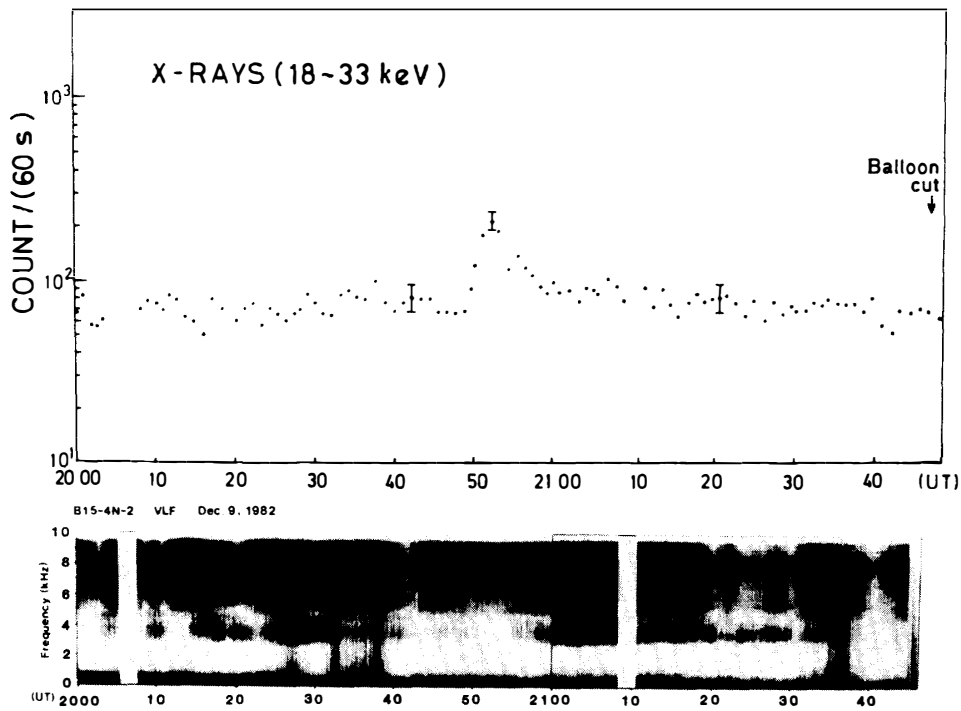


Fig. 12. Time variations of counting rates of the lower energy X-rays (18–33 keV) and dynamic spectra of the VLF emissions (0.05–10 kHz) simultaneously observed aboard the balloon B₁₅-4N on December 9, 1982. During 2050–2055 UT, a small X-ray enhancement responds to an absorption of the chorus emissions of 3–4 kHz.

chorus waves abruptly disappear at 2050–2055 UT when the counting rates of X-rays peaked. This is the first evidence showing the simultaneous on-board observations of both the electron precipitation to the ionosphere and the disappearance of VLF waves. X-ray enhancements due to precipitating energetic electrons introduce a possible increment of electron density in the ionosphere. Whereas, the logarithmic integrated absorption loss of VLF waves in the ionosphere is directly proportional to the electron density in the ionosphere (RAWER and SUCHY, 1967). The chorus waves are believed to propagate from the equatorial region in the magnetosphere to an observation site on the earth along the magnetic lines of force connecting the both (*e.g.*, BURTON and HOLZER, 1974). So, the chorus waves are interpreted to be absorbed in the ionosphere over the balloon position. It is directly revealed by the present balloon experiment that the chorus waves are strongly absorbed owing to some increase of electron density in the ionosphere.

Acknowledgments

This balloon campaign was organized by the National Institute of Polar Research under the international cooperations with Swedish and Norwegian balloon groups. Many thanks are due to the staff of the balloon flight facilities at Esrang, Sweden.

References

- BURTON, R. K. and HOLZER, R. E. (1974): The origin and propagation of chorus in the magnetosphere. *J. Geophys. Res.*, **79**, 1014–1023.
- GOLDBERG, R. A., BARCUS, J. R. and TREINISH, L. A. (1982): Mapping of auroral X-rays from rocket overflights. *J. Geophys. Res.*, **87**, 2509–2524.
- HIRASIMA, Y., MURAKAMI, H., OKUDAIRA, K., FUJII, M., NISHIMURA, J., YAMAGAMI, T. and KODAMA, M. (1983): Image-forming detectors to observe fine spatial distributions of auroral X-rays. *Mem. Natl Inst. Polar Res., Spec. Issue*, **26**, 169–179.
- KODAMA, M. and OGUTI, T. (1976): Spatial distributions of auroral zone X-rays as viewed from rocket altitudes. *Mem. Natl Inst. Polar Res., Ser A (Aeronomy)*, **14**, 1–58.
- LIN, C. S. and HOFFMAN, R. (1979): Characteristics of inverted-V events. *J. Geophys. Res.*, **84**, 1514–1524.
- MAUK, B. M., CHIN, J. and PARKS, G. (1981): Auroral X-ray images. *J. Geophys. Res.*, **86**, 6827–6835.
- MOZER, F. S. (1980): On the lowest altitude S3-3 observations of electrostatic shocks and parallel electric fields. *Geophys. Res. Lett.*, **7**, 1097–1098.
- ONO, T., MIYAOKA, H. and EJIRI, M. (1984): Spectral characteristics of VLF emissions observed by B₁₅-4N balloon launched from Esrang in Sweden. *Mem. Natl Inst. Polar Res., Spec. Issue*, **31**, 156–168.
- PARKS, G. K. (1967): Spatial characteristics of auroral zone X ray microbursts. *J. Geophys. Res.*, **72**, 215–226.
- PARKS, G. K., LIN, C. S., MAUK, B., DEFOREST, S. and McILWAIN, C. E. (1977): Characteristics of magnetospheric particle injection deduced from events observed on August 18, 1974. *J. Geophys. Res.*, **82**, 5208–5214.
- RAWER, K. and SUCHY, K. (1967): Radio-observations of the ionosphere. *Handb. Phys.*, **XLIX/2**, 383.
- YAMAGAMI, T., FUJII, M., NISHIMURA, J., MURAKAMI, H., HIRASIMA, Y., KAJIWARA, M., OKUDAIRA, K. and KODAMA, M. (1978): Balloon observations of auroral X-ray in Canada. I. Deter-

- mination of auroral X-ray illuminating region. *J. Geomagn. Geoelectr.*, **30**, 663–682.
- YAMAGISHI, H., ONO, T., FUKUNISHI, H., YAMAGAMI, T., NISHIMURA, J., KODAMA, M., HIRASIMA, Y., MURAKAMI, H., HOLTET, J. A., ULLALAND, S. and PELLINEN, R. (1984): Auroral zone X-ray pulsations associated with VLF pulsations; B₁₅-3N balloon experiment. *Mem. Natl Inst. Polar Res., Spec. Issue*, **31**, 124–136.

(Received March 21, 1984; Revised manuscript received April 17, 1984)